ACS APPLIED MATERIALS & INTERFACES

www.acsami.org

Research Article

Exploring Bonding Configurations in $MnBi_2Te_4$-Type Materials

Romakanta Bhattarai and Trevor David Rhone*

Cite This: *ACS Appl. Mater. Interfaces* 2024, 16, 60856−60864

Read Online

ACCESS | Metrics & More | Article Recommendations | Supporting Information

ABSTRACT: We perform a systematic investigation of several crystal structures, based on monolayer $MnBi_2Te_4$, of the form $MnB^iB^{ii}X^i{}_2X^{ii}{}_2$ using first-principles calculations. Our analysis shows that the most energetically favorable bonding configuration of the constituent elements in monolayer $MnB^iB^{ii}X^i{}_2X^{ii}{}_2$ is determined by the bond length between the Mn atom and its nearest X-site atoms. Tuning the bonding configuration of the material alters the magnetic, electronic, and topological properties. We also calculate the magnetic exchange parameters and magnetic anisotropy energy of the predicted structures. The calculations show that the elements at the X sites mainly determine the magnetic properties. Finally, we propose a stable phase of monolayer $MnBi_2S_2Te_2$ (i.e., γ-$MnBi_2S_2Te_2$) that exhibits the quantum anomalous Hall effect (QAHE). This study demonstrates that the bonding configuration of $MnBi_2Te_4$-type materials provides avenues for tuning the magnetic, electronic, and topological properties of van der Waals (vdW) materials.

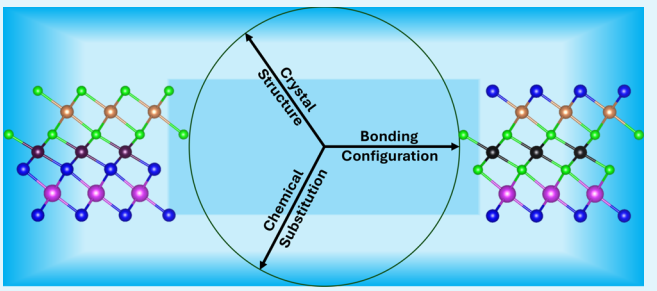

KEYWORDS: *density functional theory, 2D magnetic materials, bonding configurations, topological materials, monolayer $MnBi_2Te_4$ family, QAHE*

INTRODUCTION

One of the most peculiar features that two-dimensional (2D) materials possess is the existence of weak interlayer interactions that facilitate their exfoliation into individual atomic layers. van der Waals (vdW) magnets have received immense attention because of their novel magnetic, and topological properties such as long-range magnetic ordering, and the quantum anomalous Hall effect (QAHE).[1−7] In particular, the change in the number of layers of the vdW materials results in significant changes in their properties. Consequently, vdW materials are promising candidates for enabling the next generation of functional devices.[8] Recently, intrinsic long-range magnetic ordering in 2D materials such as $MnBi_2Te_4$ (MBT),[9,10] $Cr_2Ge_2Te_6$,[11] $MnSe_2$,[12] CrI_3,[13] Fe_3GeTe_2,[14] and $FePS_3$[15] has been discovered. vdW magnets are a platform for understanding magnetism in reduced dimension and have potential applications in spintronics, memory devices, quantum computing, and dissipationless electronics.[16−20]

MBT is the first ever experimentally verified vdW antiferromagnetic material with nontrivial topological order.[9,10] Its bulk phase consists of ABC stacked septuple layers (SL) of Bi, Mn, and Te in the following order: Te−Bi−Te−Mn−Te−Bi−Te, where each SL can be exfoliated into monolayer MBT. The ground state of MBT prefers to have an intralayer ferromagnetic spin configuration with a magnetic moment of 5 μ_B per unit cell along with an out-of-plane magnetic easy axis. Meanwhile, any two SLs are antiferromagnetically ordered. It also exhibits several nontrivial phases such as Weyl semimetal,[6] QAH insulator,[4,21] and axion insulator[22] phases. A handful of MBT-type materials have been discovered in the past including $MnBi_2Se_4$,[23−25] $MnSb_2Te_4$,[24,25] $MnSb_2Se_4$,[25,26] $MnSbBiTe_4$,[27] $MnSbBiSe_2Te_2$,[28] $MnBi_2S_2Te_2$,[29,30] and $MnBi_2Se_2Te_2$.[29,30] Recently, a data-driven study investigated several Janus and non-Janus MBT-type materials including the competing phases of some of the aforementioned materials.[31] These studies show that the properties of MBT-type materials depend on their chemical composition.

The existence of multiple atomic layers in monolayer MBT-type materials provides a unique platform for rearranging the atomic layers to form different structures with varying properties. At the same time, however, it also imposes challenges for determining which bonding sequence is most energetically favorable. Although several phases of the MBT-type monolayers have been investigated in the past, it is not clear whether they are the most stable phases in that particular system. Examples include monolayers of $MnBi_2S_2Te_2$, $MnBi_2Se_2Te_2$, and $MnSbBiSe_2Te_2$ where only a specific bonding sequence has been explored.[28−30] We address this challenge by performing a systematic case study of MBT-type

Received: August 1, 2024
Revised: October 18, 2024
Accepted: October 22, 2024
Published: October 29, 2024

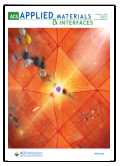

https://doi.org/10.1021/acsami.4c12946
ACS Appl. Mater. Interfaces 2024, 16, 60856−60864

materials. We expect that our study will provide an understanding of bonding configuration in MBT-type materials that may motivate researchers to revisit other vdW materials that possess multiple bonding arrangements.

In this study, we perform a systematic investigation of several possible phases of ten different MBT-type monolayers. We find that there is a common favorable bonding configuration among all $MnB^iB^{ii}X^i_2X^{ii}_2$ structures considered in this work. This configuration is based on the bond length between the Mn atom and its nearest X-site atoms that make chemical bonds with Mn. The most favorable configuration tends to have shorter bond lengths between the Mn atom and its nearest X-site atoms. This is only possible if the element occupying the X-sites nearest to Mn is smaller than those further away. In addition, changing the bonding configuration of these materials can impact the formation energy and the electronic properties. For instance, a transition from metal to trivial insulator, and Chern insulator can occur. We investigate the thermodynamic, electronic, magnetic, and topological properties of monolayer $MnB^iB^{ii}X^i_2X^{ii}_2$ for the most favorable configurations. Finally, we propose a high-energy phase of the $MnBi_2S_2Te_2$ structure (i.e., γ-$MnBi_2S_2Te_2$) that is chemically stable (i.e., via thermodynamic and dynamic stability checks) and exhibits a QAHE.

RESULTS AND DISCUSSION

Figure 1 shows the crystal structure of monolayer $MnB^iB^{ii}X^i_2X^{ii}_2$ with ferromagnetic (FM) and antiferromagnetic

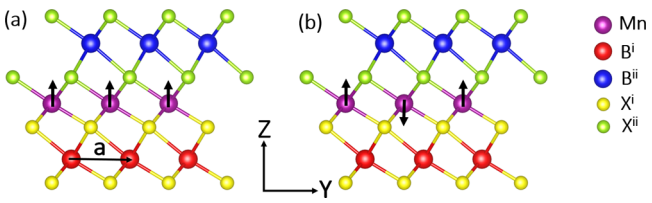

Figure 1. Crystal structure of the $MnBi_2Te_4$-type monolayer. The structure represents one of the possible structural configurations of monolayer $MnB^iB^{ii}X^i_2X^{ii}_2$. It has the following atomic sequence from top to bottom: X^{ii}-B^{ii}-X^{ii}-Mn-X^i-B^i-X^i. (a) and (b) represent the FM and AFM states, respectively.

(AFM) spin configurations. The B sites of $MnB^iB^{ii}X^i_2X^{ii}_2$ (i.e., B^i and B^{ii}) are decorated with Bi (i.e., Bi_2), or Sb (i.e., Bi_2), or both of them (i.e., SbBi). Similarly, the X sites (i.e., X^i and X^{ii}) can be either S, Se, or Te (i.e., S_4, Se_4, Te_4), or a combination of two of them (i.e., S_2Se_2, S_2Te_2, Se_2Te_2). In this study, we consider 10 different materials that are isostructural to the monolayer of MBT. The competing phases of some of these structures are already predicted in previous studies.[28−31] For a given $MnB^iB^{ii}X^i_2X^{ii}_2$ structure, we investigate all possible arrangements of the elements occupying the A, B, and X sites. These bonding configurations, based on the arrangement of atoms in the septuple layer, are described by the sequence of elements in the SL. We calculate the total energy and electronic band gap of each configuration and compare these values with those from the respective competing phases. See Supporting Information for details.

We propose notation symbols for the different phases of monolayer $MnB^iB^{ii}X^i_2X^{ii}_2$ structures based on their atomic sequences in the crystal structure. For those with the same B site elements (i.e., B_2 = Bi_2, Bi_2), there will be four possible sequences (i.e., α, β, γ, and δ). For example, in $MnBi_2S_2Se_2$ those four names are as follows: α-$MnBi_2S_2Se_2$ (with atomic sequence: S−Bi−Se−Mn−Se−Bi−S), β-$MnBi_2S_2Se_2$ (with atomic sequence: Se−Bi−S−Mn−S−Bi−Se), γ-$MnBi_2S_2Se_2$ (with atomic sequence: Se−Bi−S−Mn−Se−Bi−S), and δ-$MnBi_2S_2Se_2$ (with atomic sequence: Se−Bi−Se−Mn−S−Bi−S). Similar pattern holds for monolayers of $MnBi_2S_2Te_2$, $MnBi_2Se_2Te_2$, $MnSb_2S_2Se_2$, $MnSb_2S_2Te_2$, and $MnSb_2Se_2Te_2$. For those with both Sb and Bi at the B sites (i.e., B_2 = BiSb), there will be six possible sequences (i.e., α, β, γ, δ, ϵ, and ζ). For example, in $MnSbBiS_2Se_2$ those six names are as follows: α-$MnSbBiS_2Se_2$ (with atomic sequence: S−Sb−Se−Mn−Se−Bi−S), β-$MnSbBiS_2Se_2$ (with atomic sequence: Se−Sb−S−Mn−S−Bi−Se), γ-$MnSbBiS_2Se_2$ (with atomic sequence: Se−Sb−S−Mn−Se−Bi−S), δ-$MnSbBiS_2Se_2$ (with atomic sequence: S−Sb−Se−Mn−S−Bi−Se), ϵ-$MnSbBiS_2Se_2$ (with atomic sequence: Se−Sb−Se−Mn−S−Bi−S), and ζ-$MnSbBiS_2Se_2$ (with atomic sequence: S−Sb−S−Mn−Se−Bi−Se). This pattern also holds for monolayers of $MnSbBiS_2Te_2$, and $MnSbBiSe_2Te_2$. A detailed table of all $MnB^iB^{ii}X^i_2X^{ii}_2$ structures is provided in the Supporting Information along with the representative crystal structures of each type, namely, monolayers of $MnBi_2S_2Se_2$ and $MnSbBiS_2Se_2$.

We determine the most favorable atomic sequence for monolayer $MnB^iB^{ii}X^i_2X^{ii}_2$ materials by identifying the lowest energy configuration. We observe that the elements occupying the X sites (i.e., X^i, and X^{ii}) are responsible for determining the ground states of $MnB^iB^{ii}X^i_2X^{ii}_2$ structures. For example, among the four possible atomic sequences in monolayer $MnBi_2S_2Se_2$, we find that the structure with atomic sequence Se−Bi−S−Mn−S−Bi−Se (i.e., β-phase) has the lowest energy configuration, suggesting that the magnetic atom (i.e., Mn) in $MnBi_2S_2Se_2$ prefers to have chemical bonds with the atoms in the X sites that are smaller in atomic size (i.e., S) than those occupying the X sites on the surface (i.e., Se). In other words, a structure comprising S (Se) and Se (Te) atoms on the X sites will always have S (Se) atoms chemically bonded to the Mn atoms and Se (Te) atoms on the surface bonded to the B-site atoms. A similar pattern is observed for structures comprising S and Te atoms on the X sites. This holds for all MBT-type structures considered in this study. In other words, the atoms in $MnB^iB^{ii}X^i_2X^{ii}_2$ structures prefer to be arranged in the sequence of the β-phase. Thus, $MnB^iB^{ii}X^i_2X^{ii}_2$ structures comprise a MnX^i_2 layer at the center of the cell with two inverted layers: B^iX^{ii}, and $B^{ii}X^{ii}$, as the top and bottom layers.

This study demonstrates that the MBT family of materials prefers to have a centrosymmetric structure whenever possible. If the centrosymmetry condition is not satisfied, they still prefer to have the X-sites near the Mn-sites be smaller than those near the surface. Thus, $MnB^iB^{ii}X^i_2X^{ii}_2$ materials that do not satisfy the above conditions are high-energy phases. Consequently, we find that materials, such as δ-$MnBi_2S_2Te_2$, δ-$MnBi_2Se_2Te_2$, ϵ-$MnSbBiS_2Te_2$, and ζ-$MnSbBiSe_2Te_2$, which are reported in previous studies[28−31] are the higher-energy competing phases of the structures predicted in this work. See Supporting Information for details.

To better understand how the atomic configuration in monolayer $MnB^iB^{ii}X^i_2X^{ii}_2$ materials affects the energy of the phase, we analyze the bond distances between all atomic pairs that share a common chemical bond in the structures. That is, we measure the following bond distances: Mn−X^i, Mn−X^{ii}, B^i−X^i, and B^{ii}−X^{ii}. We find that the Mn−X^i bond is always shorter when X^i is a chalcogen with a smaller atomic number.

https://doi.org/10.1021/acsami.4c12946
ACS Appl. Mater. Interfaces 2024, 16, 60856−60864

i.e., Mn−S is the smallest and the Mn−Te is the largest Mn−X^i bond distance in $MnB^iB^{ii}X^i_2X^{ii}_2$ structures. The structures that have atomic configurations with shorter Mn-X^i bonds are energetically favorable. This holds for all the structures considered in our study. A table of Mn−X^i bond lengths is provided in Supporting Information.

A list of all the predicted structures in their most energetically favorable atomic arrangements (i.e., β-phase) along with their corresponding formation energies per unit cell and electronic band gaps are presented in Table 1. We find that the formation energy of MBT-type structures depends on the selection of elements occupying the atomic sites, with B sites being the most important. For example, the formation energy per unit cell of monolayer β-$MnBi_2S_2Se_2$ (i.e., −2.759 eV) is much lower than that of monolayer β-$MnSb_2S_2Se_2$ (i.e., −1.038 eV). In addition, for a fixed B site, the structures comprising X sites as the combination of S, Se, (i.e., S_2Se_2) and Se, Te (i.e., Se_2Te_2) have lower formation energies per unit cell than those structures with S, Te (i.e., S_2Te_2). We use the formation energy as a proxy for the chemical stability of the predicted structures. Nevertheless, the formation energy is a necessary, but insufficient condition for chemical stability. The materials with lower formation energies are thermodynamically more stable. Consequently, we deduce that monolayer β-$MnBi_2S_2Se_2$ has the highest thermodynamic stability among all the structures considered in this study. Meanwhile, monolayer β-$MnSb_2S_2Te_2$ has the lowest thermodynamic stability.

Table 1. $MnB^iB^{ii}X^i_2X^{ii}_2$ Structures with their Chemical Formulae, Most Favorable Atomic Sequences, Corresponding Formation Energies per Unit Cell, and Band Gap Values

material	atomic arrangement	formation energy (eV/unit cell)	band gap (eV)
β-$MnBi_2S_2Se_2$	Se−Bi−S−Mn−S−Bi−Se	−2.759	0.655
β-$MnBi_2S_2Te_2$	Te−Bi−S−Mn−S−Bi−Te	−2.281	0.578
β-$MnBi_2Se_2Te_2$	Te−Bi−Se−Mn−Se−Bi−Te	−2.389	0.386
β-$MnSb_2S_2Se_2$	Se−Sb−S−Mn−S−Sb−Se	−1.038	0.592
β-$MnSb_2S_2Te_2$	Te−Sb−S−Mn−S−Sb−Te	−0.568	0.709
β-$MnSb_2Se_2Te_2$	Te−Sb−Se−Mn−Se−Sb−Te	−0.631	0.446
β-$MnSbBiS_2Se_2$	Se−Sb−S−Mn−S−Bi−Se	−1.888	0.532
β-$MnSbBiS_2Te_2$	Te−Sb−S−Mn−S−Bi−Te	−1.418	0.587
β-$MnSbBiSe_2Te_2$	Te−Sb−Se−Mn−Se−Bi−Te	−1.503	0.363
$MnSbBiS_4$	S−Sb−S−Mn−S−Bi−S	−1.664	0.665
$MnSbBiSe_4$[31]	Se−Sb−Se−Mn−Se−Bi−Se	−1.865	0.328
$MnSbBiTe_4$[27]	Te−Sb−Te−Mn−Te−Bi−Te	−1.718	0.237

To determine the dynamic stability of the predicted structures, we carry out phonon calculations using the finite displacement method as implemented in the Phonopy package.[32] Larger supercells of size 4 × 4 × 1 are considered in the calculations. We find that there are no imaginary phonon frequencies in the phonon spectra. The absence of soft vibration modes in the phonon spectra of lowest energy $MnB^iB^{ii}X^i_2X^{ii}_2$ structures provides evidence that they are dynamically stable. The calculated phonon spectra of all the predicted structures are provided in the Supporting Information.

We investigate the electronic properties of monolayer $MnB^iB^{ii}X^i_2X^{ii}_2$ structures for the most favorable bonding configurations. Table 1 presents the DFT-calculated band gap values. All the structures are found to be trivial insulators with nonzero band gaps. To get a deeper insight into the electronic properties, we plot their electronic band structures and projected density of states (PDOS) based on the elemental contributions. The corresponding plots of β-$MnBi_2S_2Se_2$ and β-$MnSbBiSe_2Te_2$ monolayers are shown in Figure 2. The plots of their total DOS are provided in the Supporting Information along with the electronic band structures of monolayer $MnB^iB^{ii}X^i_2X^{ii}_2$ structures.

We find that the band structure and projected DOS of both monolayers show a clear separation of the valence band (VB) and conduction band (CB) indicating insulating behavior. The projected DOS of β-$MnBi_2S_2Se_2$ monolayer (Figure 2a) shows that S and Se have a major contribution to the VB near the Fermi level, while Bi and Se have a major contribution to the CB near the Fermi level. The contribution of Mn near the Fermi level is negligible. Similarly, the projected DOS of β-$MnSbBiSe_2Te_2$ monolayer (Figure 2b) shows that Se and Te are the major contributors to both the VB and CB near E_F. There is a small contribution coming from Sb and Bi to the CB near E_F. Meanwhile, Mn has a negligible contribution near E_F as in Figure 2a. Similar patterns are observed in other MBT-type materials considered in this study. This suggests that the extremely localized 3d-orbitals of Mn atoms are not responsible for determining the electronic band gaps of $MnB^iB^{ii}X^i_2X^{ii}_2$ monolayers.

Next, we investigate the magnetic properties of monolayer $MnB^iB^{ii}X^i_2X^{ii}_2$ structures using the isotropic Heisenberg Hamiltonian,

$$H = -J \sum_{i,j} S_i \cdot S_j - A \sum_i (S_i^z)^2 \quad (1)$$

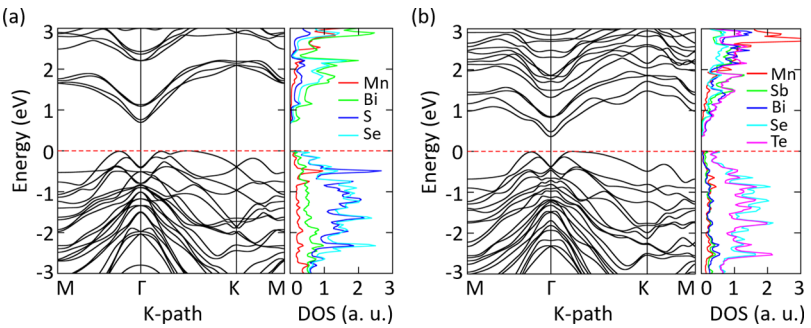

Figure 2. Band structure and element-decomposed density of states of (a) β-$MnBi_2S_2Se_2$ monolayer, and (b) β-$MnSbBiSe_2Te_2$ monolayer. The spin−orbit interaction is included in the calculations.

https://doi.org/10.1021/acsami.4c12946
ACS Appl. Mater. Interfaces 2024, 16, 60856−60864

where J is the Heisenberg exchange coupling parameter, A measures the strength of the single-ion anisotropy, S_i and S_j represent the neighboring spin unit vectors at site i and j, respectively. In this study, we calculate the first, second, and third nearest-neighbor exchange interactions that are represented by J_1, J_2, and J_3 respectively. For this, we use a supercell of size 3 × 2 × 1 with four possible magnetic configurations, as

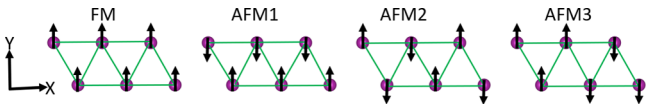

Figure 3. Magnetic configurations in monolayer $MnB^iB^{ii}X^i_2X^{ii}_2$. Schematic shows one FM and three AFM magnetic configurations in a 3 × 2 × 1 supercell of monolayer $MnB^iB^{ii}X^i_2X^{ii}_2$. Only the magnetic Mn atoms are displayed.

shown in Figure 3. The magnetic exchange coupling parameters are obtained by solving the following equations[28]:

$$E_{FM} = E_0 - 18(J_1 + J_2 + J_3)S^2$$
$$E_{AFM1} = E_0 - 6(-J_1 - J_2 + 3J_3)S^2$$
$$E_{AFM2} = E_0 - 2(-3J_1 + J_2 + J_3)S^2$$
$$E_{AFM3} = E_0 - 2(-J_1 - 3J_2 + J_3)S^2 \quad (2)$$

Where E_0 is the ground state energy that does not depend upon the spin configurations. The calculated values of J_1, J_2, and J_3 are presented in Table 2. The positive (negative) J values represent the FM (AFM) spin configuration. We also calculate the magnetic anisotropy energy (MAE), which is the sum of the magnetocrystalline anisotropy (MCA) energy and the magnetic shape anisotropy (MSA) energy. The MCA energy emerges from the spin−orbit interaction and is calculated by taking the energy difference between the in-plane (IP) and out-of-plane (OOP) spin configurations, MCA = $E_{IP} - E_{OOP}$. The MSA energy originates from the long-range magnetic dipole−dipole interactions.[33,34] It is calculated using the formula, MSA = $E^{Dipole}_{IP} - E^{Dipole}_{OOP}$. Positive (negative) values of MAE indicate that the magnetic moments prefer to align in the OOP (IP) direction. See Supporting Information for details.

We find that the first nearest neighbor exchange interaction in monolayer $MnB^iB^{ii}X^i_2X^{ii}_2$ always prefers ferromagnetic ordering, while the second and third nearest neighbors tend to prefer the AFM spin configuration. Supporting evidence, as shown in Table 2, finds J_1 with positive values while J_2, and J_3 have negative values. J_1 is strongest for structures with Se and Te and lowest for those with S and Te. Among the structures considered in this study, we find that $MnSbBiSe_4$ has the highest J_1 and $MnSbBiS_4$ has the lowest J_1. The corresponding values are 1.294 and 0.546 meV, respectively. Magnitude of J_2 is largest for $MnBi_2Se_2Te_2$ (i.e., −0.132 meV) and lowest for $MnSb_2S_2Te_2$ (i.e., −0.064 meV). Surprisingly, the value of J_3 for β-$MnSb_2S_2Se_2$ is higher than that of J_2. i.e., the third nearest-neighbor interaction is dominant over the second nearest-neighbor interaction. We expect that if the higher-order exchange coupling parameters prefer AFM configurations and are significant as compared to J_1, there might be a possibility of spin frustration in MBT-type materials. Similar results have been reported in previous studies.[35,36] In addition, the exchange-coupling parameters of vdW materials can be tuned by applying external perturbations such as chemical doping, electric field, or strain.[28,29,35,37−39] Changing the coupling parameters may lead to spin frustration in $MnB^iB^{ii}X^i_2X^{ii}_2$ structures. However, investigating spin frustration is outside the scope of this work.

The dipole−dipole interaction usually favors the in-plane magnetization as shown by negative MSA values in Table 2. Meanwhile, MCA can be either positive or negative. Table 2 shows that $MnB^iB^{ii}X^i_2X^{ii}_2$ monolayers always have negative MCA energy if their X-sites comprise a combination of S and Se (i.e., S_2Se_2) and have positive MCA for Se and Te at the X sites. For those with S and Te, MCA is almost zero. This suggests that the identity of the X-sites determines the MCA energy of $MnB^iB^{ii}X^i_2X^{ii}_2$ monolayers. The role of X-site elements is also crucial in determining the magnitude of magnetic exchange coupling parameters and MAE in other vdW magnets, such as $Cr_2Ge_2Te_6$, CrI_3, and $MnSe_2$. Studies show that these materials tend to have larger (in magnitude) exchange coupling parameters, and MAE for the structures with larger elements at the X sites.[19,20,40−45]

For monolayer MBT, MCA is positive and it dominates MSA[39] making out-of-plane magnetic easy axis. However, an opposite trend is observed in other materials, such as $MnBi_2Se_4$[23] where MCA is very low compared with MSA, resulting in an in-plane magnetization. We find a similar pattern in this study; the calculated MAE energies show that all the structures we investigate in this work have weak MCA that are dominated by strong MSA values. As a result, all

Table 2. Magnetic Properties of Monolayer $MnB^iB^{ii}X^i_2X^{ii}_2$ Structures in their Lowest Energy States[a]

material	magnetic moment (μ_B)	J_1 (meV)	J_2 (meV)	J_3 (meV)	MCA (meV)	MSA (meV)	MAE (meV)
β-$MnBi_2S_2Se_2$	4.661	0.732	−0.120	−0.043	−0.021	−0.168	−0.189
β-$MnBi_2S_2Te_2$	4.660	0.695	−0.100	−0.004	0.013	−0.156	−0.143
β-$MnBi_2Se_2Te_2$	4.645	1.030	−0.132	−0.006	0.030	−0.146	−0.143
β-$MnSb_2S_2Se_2$	4.652	0.690	−0.108	−0.176	−0.097	−0.179	−0.276
β-$MnSb_2S_2Te_2$	4.651	0.642	−0.064	−0.049	−0.001	−0.164	−0.165
β-$MnSb_2Se_2Te_2$	4.635	1.195	−0.092	−0.028	0.037	−0.154	−0.117
β-$MnSbBiS_2Se_2$	4.655	0.726	−0.115	−0.084	−0.016	−0.174	−0.190
β-$MnSbBiS_2Te_2$	4.655	0.681	−0.084	−0.011	0.004	−0.160	−0.156
β-$MnSbBiSe_2Te_2$	4.640	1.126	−0.114	−0.001	0.034	−0.150	−0.116
$MnSbBiS_4$	4.652	0.546	−0.119	−0.097	≈0	−0.182	−0.182
$MnSbBiSe_4$	4.639	1.294	−0.123	−0.071	0.024	−0.135	−0.111

[a]Total magnetic moment, exchange coupling parameters, MAE, and magnetic easy axis are displayed.

https://doi.org/10.1021/acsami.4c12946
ACS Appl. Mater. Interfaces 2024, 16, 60856−60864

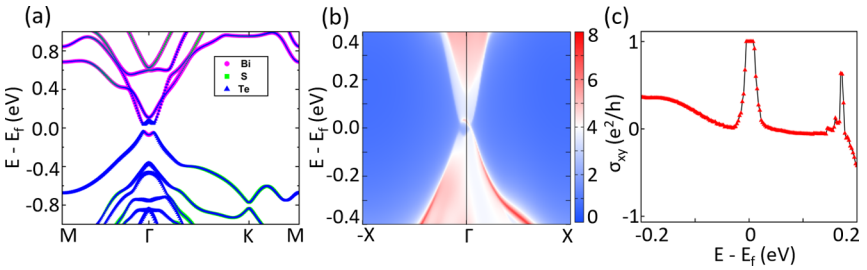

Figure 4. Topological properties of monolayer γ-$MnBi_2S_2Te_2$. (a) element-decomposed band structure, (b) edge states, and (c) Hall conductance of monolayer γ-$MnBi_2S_2Te_2$.

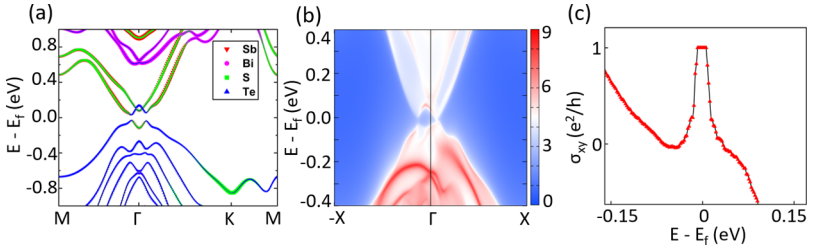

Figure 5. Topological properties of ξ-$MnSbBiS_2Te_2$ monolayer. (a) element-decomposed band structure, (b) edge states, and (c) Hall conductance of ξ-$MnSbBiS_2Te_2$ monolayer.

$MnB^iB^{ii}X^i{}_2X^{ii}{}_2$ structures considered in our study prefer to have an in-plane magnetization.

Finally, we study the topological properties of $MnB^iB^{ii}X^i{}_2X^{ii}{}_2$ monolayers. Some of the structures such as ζ-$MnSbBiSe_2Te_2$, ϵ-$MnSbBiS_2Te_2$, δ-$MnBi_2S_2Te_2$, and δ-$MnBi_2Se_2Te_2$[28−30,46] were predicted to possess nontrivial topological states. A previous study by You et al. shows that δ-$MnBi_2S_2Te_2$ monolayer exhibits QAHE with the Chern number C = 2. This structure has an atomic arrangement in the following order: S−Bi−S−Mn−Te−Bi−Te. In this study, we find two previously unexplored phases of $MnB^iB^{ii}X^i{}_2X^{ii}{}_2$ that exhibit topological features. Our analysis shows that changing the atomic sequence to Te−Bi−S−Mn−Te−Bi−S results in a new phase (i.e., γ-$MnBi_2S_2Te_2$) with the formation energy of −1.898 eV per unit cell. This value is lower than that of the previously proposed δ-$MnBi_2S_2Te_2$ which has a formation energy of −1.869 eV per unit cell. This implies that the newly predicted γ-$MnBi_2S_2Te_2$ phase is energetically more stable than the previously reported phases. The dynamic stability of the γ-$MnBi_2S_2Te_2$ is further tested by calculating the phonon spectrum and the ab initio molecular dynamics (AIMD) simulations within the NVT ensemble at 500 K for 30 ps with a time step of 2 fs. The absence of imaginary frequencies in the phonon spectrum that would indicate soft phonon modes is evidence of dynamic stability. In addition, the AIMD result shows no sudden drop of fluctuating total energy in the energy profile over the simulation period of 30 ps. This suggests that the structure is dynamically stable. See Supporting Information for details. The electronic structure calculations show that the γ-$MnBi_2S_2Te_2$ has a direct band gap of 80.3 meV near the Γ point. The corresponding element-decomposed band structure is shown in Figure 4a. It shows a clear band inversion at the Γ point indicating topologically nontrivial features.

To confirm this, we calculate the topological constant using the Z_2Pack package, which shows that γ-$MnBi_2S_2Te_2$ monolayer is a Chern insulator with a Chern number C = 1 which exhibits QAHE. The Chern insulating phase of γ-$MnBi_2S_2Te_2$ monolayer is further confirmed by calculating the edge states using the WannierTools package as shown in Figure 4b. It features a gapless chiral edge state connecting the valence bands and conduction bands. We also calculate the anomalous Hall conductivity σ_{xy}, which is shown in Figure 4c. The Hall conductivity is quantized with a Hall plateau of $\frac{e^2}{h}$ at the Fermi level corresponding to a Chern number C = 1, thus indicating a QAH state.

In addition, a recent study predicts that the ϵ-$MnSbBiS_2Te_2$ monolayer undergoes a phase transition from metallic to Chern insulating phase with C = 2 when a biaxial strain is applied.[46] The atomic ordering of this phase is found to be Te−Sb−Te−Mn−S−Bi−S with a formation energy of −1.063 eV per unit cell. When we alter the order of the atomic sequence, we obtain an additional phase (i.e., ζ-$MnSbBiS_2Te_2$) that also exhibits QAHE without applying strain. It has an atomic ordering of S−Sb−S−Mn−Te−Bi−Te and a formation energy of −0.897 eV per unit cell. The topologically nontrivial behavior is confirmed using the Z_2Pack and WannierTools packages. The results show that the ζ-$MnSbBiS_2Te_2$ phase exhibits QAHE with a Chern number C = 1. The corresponding element-decomposed band structures with band inversion at Γ point, chiral edge states, and quantized anomalous Hall conductivity are shown in Figure 5. However, results from the phonon spectrum calculations show that the newly predicted ζ-$MnSbBiS_2Te_2$ phase is dynamically unstable or at least metastable. See Supporting Information for its phonon spectrum. This instability might suggest the possible surface reconstruction in the ζ-$MnSbBiS_2Te_2$ structure after exfoliation from the bulk. We may be able to get rid of those soft modes by using larger supercells in the phonon calculations that are sufficient to capture the reconstructed surfaces correctly. A paper by Ramzan et al. discussed the possible scenarios of surface reconstruction in vdW materials of the form XY_3 (X = C, Si, Ge, Sn, Pb; Y = P, As, Sb, Bi). The authors chose slightly distorted rectangular cells over regular hexagonal cells in the calculations to overcome this issue in such systems.[47] It may also be possible to induce dynamic stability in the ζ-$MnSbBiS_2Te_2$ phase by adding a second layer

https://doi.org/10.1021/acsami.4c12946
ACS Appl. Mater. Interfaces 2024, 16, 60856−60864

as a substrate or by hydrogenation. Studies demonstrating this have been reported in the literature.[48−59] It should be noted that both phases discussed above are the high-energy competing phases of our previously predicted most-stable $MnB^{i}B^{ii}X^{i}_{2}X^{ii}_{2}$ structures in Table 1.

It is well-known that the standard DFT method using GGA-PBE functional underestimates the band gap. A few approaches have been proposed to overcome this problem, such as using the DFT + U method,[60] hybrid functionals,[61,62] green function GW,[63−65] and Bethe Salpeter Equation (BSE) methods.[66,67] We use the DFT + U method with U = 4 eV in our calculations. The value of U is taken from the literature.[6,25,27,28,31,46,68,69] This method has been widely used to calculate the properties of MBT-type materials because it predicts their properties accurately. Previous studies have tested the DFT + U method with different values of the U parameters as well as the higher-order functionals such as the HSE method on MBT-type materials and found that all of them led to the same results qualitatively. The study also found that the standard DFT method (i.e., with U = 0 eV) results in monolayer MBT-type materials relaxing to the wrong magnetic configuration.[9,27,46] We also calculate the band gaps of monolayers γ-$MnBi_2S_2Te_2$ and ζ-$MnSbBiS_2Te_2$, that are predicted to exhibit QAHE, using the DFT + U method taking different U values as well as the HSE method. The calculations show that while the values of the band gap change slightly with the different functionals used, the topological properties remain unchanged. Our results are thus consistent with the previous studies.[9,27,46] See Supporting Information for details.

Our study provides a comprehensive understanding of various possible phases of monolayer $MnB^{i}B^{ii}X^{i}_{2}X^{ii}_{2}$ structures. It shows how the stability of $MnB^{i}B^{ii}X^{i}_{2}X^{ii}_{2}$ materials, as well as their electronic, magnetic and topological properties, can be altered by rearranging the sequence of elements occupying the A, B, and X sites of the material. In addition, the calculations show that the most stable phases of monolayer $MnB^{i}B^{ii}X^{i}_{2}X^{ii}_{2}$ structures are energetically preferred by a few hundred meV, ranging from 148 meV (for monolayer $MnSbBiS_2Se_2$) to 788 meV (for monolayer $MnSb_2S_2Te_2$) as compared to their respective high-energy competing phases. This shows that the competing phases are metastable phases of the respective structures. Previous studies show that it is feasible to grow the competing phases of various vdW materials that have the same chemical composition but different stacking sequences by using proper growth conditions. For example, Bao et al. in 2012 and Martínez-Velarte et al. in 2017 experimentally synthesized quintuple layers Bi_2TeSe_2 structure using the Bridgman technique where atoms are arranged in a disordered occupation of Te/Se on outer quintuple layers and Se atoms are located at the central-layer in the following order: Se/Te−Bi−Se−Bi−Se/Te.[70,71] Choi et al. in 2015 used the thermal evaporation method to synthesize a centrosymmetric Bi_2TeSe_2 structure with a stacking sequence of the Se−Bi−Te−Bi−Se quintuple-layer unit.[72] Later in 2024, Jou et al. also successfully synthesized a Janus Bi_2TeSe_2 structure with a stacking sequence of the Se−Bi−Se−Bi−Te using the vdW epitaxy method.[73] The Above phases are the competing phases of Bi_2TeSe_2 with different atomic sequences. Thus, we expect that the competing phases of $MnB^{i}B^{ii}X^{i}_{2}X^{ii}_{2}$ structures identified in our work can also be realized in the experiments with proper growth conditions - that is optimal temperature, pressure, composition, and other relevant synthesis conditions.[9,10,70−72,74]

As per an experimental paper by Gong et al., MBT films can be fabricated in an SL-by-SL manner by alternate growth of 1 quintuple layer of Bi_2Te_3 and 1 bilayer of MnTe with the molecular beam epitaxy (MBE) method.[10] Based on the above references, we surmise that it is possible to grow the respective bulk phases of MBT-type materials by using one of the methods described above. One can first grow bulk $MnB^{i}B^{ii}X^{i}_{2}X^{ii}_{2}$, then exfoliate it into a single layer. Alternatively, these monolayers can be grown in quintuple layers of $B^{i}_{2}X^{i}_{3}$ and $B^{ii}_{2}X^{ii}_{3}$, and bilayers of MnX^{i} or MnX^{ii} (B^{i}, B^{ii} = Bi, Sb; X^{i}, X^{ii} = S, Se, Te) via the MBE method as described by Gong et al.[10] We find that similar ideas have also been proposed in previous theoretical studies.[27,29]

Our work can be extended to investigate the electronic, magnetic, topological, and phase transition properties of other MBT monolayers, their bilayers, multilayers, and heterostructures, as well as various other layered materials not belonging to the MBT family. In addition, we identify several Janus MBT-type materials that are candidates for future investigations of piezoelectric properties.

CONCLUSIONS

In summary, we perform a systematic analysis of several phases of monolayer $MnB^{i}B^{ii}X^{i}_{2}X^{ii}_{2}$ structures, based on $MnBi_2Te_4$, using first-principles calculations. We find that the arrangement of constituent elements in the crystal structure determines its characteristics. Our analysis shows that the bond distance between the Mn atom and its nearest X-site elements is responsible for determining the ground state of $MnB^{i}B^{ii}X^{i}_{2}X^{ii}_{2}$ materials considered in the study. In addition, based on the bonding configuration, the materials will have varying electronic, magnetic, and topological properties. The magnetic exchange coupling parameters and MCA energies show that the X-site elements play a crucial role in determining the magnetic properties. Finally, we propose a stable phase of monolayer $MnBi_2S_2Te_2$ (i.e., γ-$MnBi_2S_2Te_2$) that exhibits QAHE. This study provides a framework for creating a comprehensive understanding of $MnBi_2Te_4$-type materials. This work also demonstrates that the bond engineering of $MnBi_2Te_4$-type materials provides avenues for tuning the magnetic, electronic, and topological properties of van der Waals (vdW) materials. In other words, rearranging the sequence of atoms in the septuple layer provides a novel tuning knob for designing materials. Magnetic topological materials have potential applications in spintronics, topological quantum computing, and dissipationless electronics.

METHODS

First-principles calculations are performed by using the VASP package[75] that uses projected augmented wave (PAW) potential to describe the interaction between electrons and ion cores.[76] We use the exchange and correlation functional constructed within the generalized gradient approximation in the Perdew−Burke−Ernzerhof formulation (GGA-PBE).[77] A Gamma-centered k-pint mesh of 15 × 15 × 1 is used for the integration of the Brillouin zone. To consider the effect of 3d-electrons in Mn atoms, we use a DFT+U method[60] with a value of the self-interaction term U = 4 eV in all the calculations, which is taken from the previous studies.[6] The electronic wave functions are expanded in terms of the plane wave basis sets with an energy cutoff of 500 eV. The spin−orbit interactions and spin polarization are considered in the calculations. The criterion for the electronic convergence is set to 10^{-9} eV between any two successive

https://doi.org/10.1021/acsami.4c12946
ACS Appl. Mater. Interfaces 2024, 16, 60856−60864

steps. The structures are allowed to relax until the force between any two successive ionic steps is less than 10^{-4} eV/Å. A vacuum space of nearly 30 Å is set along the *z*-direction to avoid interactions with the periodic replicas. A denser *k*-point mesh of 25 × 25 × 1 is used to calculate the magnetic anisotropy energies. The phonon dispersions are calculated using the Phonopy package.[32] The magnetic exchange parameters are calculated in larger supercells of size 3 × 2 × 1 using the Heisenberg Hamiltonian. The topological constants are calculated using the Z_2Pack package[78] and the edge states calculations are performed using the WannierTools package.[79]

■ ASSOCIATED CONTENT

Data Availability Statement

All data needed to evaluate the conclusions in the paper are present in the paper and/or the Supporting Information. Any additional data related to this paper may be provided upon reasonable request.

Supporting Information

The Supporting Information is available free of charge at https://pubs.acs.org/doi/10.1021/acsami.4c12946.

Different phases of monolayer $MnB^iB^{ii}X^i_2X^{ii}_2$ structures and their atomic arrangements, crystal structures of clusters of possible phases in $MnB^iB^{ii}X^i_2X^{ii}_2$ structures, phonon spectra of $MnB^iB^{ii}X^i_2X^{ii}_2$ structures, analysis of bond lengths between Mn and X-site atoms in monolayer $MnB^iB^{ii}X^i_2X^{ii}_2$ structures, AIMD simulation of γ-$MnBi_2S_2Te_2$ monolayer, electronic band structures of $MnB^iB^{ii}X^i_2X^{ii}_2$ structures, band structure and total DOS of β-$MnBi_2S_2Se_2$ and β-$MnSbBiSe_2Te_2$ monolayers, band gaps of monolayers γ-$MnBi_2S_2Te_2$ and ζ-$MnSbBiS_2Te_2$ using different methods, lattice constants of relaxed monolayer $MnB^iB^{ii}X^i_2X^{ii}_2$ structures in the most favorable bonding configurations, and magnetic shape anisotropy calculations of monolayer $MnB^iB^{ii}X^i_2X^{ii}_2$ structures (PDF)

■ AUTHOR INFORMATION

Corresponding Author

Trevor David Rhone − *Department of Physics, Applied Physics, and Astronomy, Rensselaer Polytechnic Institute, Troy, New York 12180, United States;* orcid.org/0000-0002-0198-9952; Email: rhonet@rpi.edu

Author

Romakanta Bhattarai − *Department of Physics, Applied Physics, and Astronomy, Rensselaer Polytechnic Institute, Troy, New York 12180, United States;* orcid.org/0000-0002-7216-8756

Complete contact information is available at: https://pubs.acs.org/10.1021/acsami.4c12946

Author Contributions

R.B. and T.D.R. conceived the idea of the project. R.B. performed the calculations and analyzed the results. R.B. and T.D.R. wrote the manuscript.

Notes

The authors declare no competing financial interest.

■ ACKNOWLEDGMENTS

This work is supported by the NSF CAREER award under grant number 2044842. The Extreme Science and Engineering Discovery Environment (XSEDE) and Advanced Cyberinfrastructure Coordination Ecosystem: Services and Support (ACCESS) provide the computational resources under the NSF grant number ACI-1548562. In addition, we use the resources of the Argonne Leadership Computing Facility, which is a DOE Office of Science User Facility supported under Contract DE-AC02-06CH11357. The authors thank Raagya Arora and Efthimios Kaxiras at Harvard University and Peter Minch at Rensselaer Polytechnic Institute for useful discussions.

■ REFERENCES

(1) Yu, R.; Zhang, W.; Zhang, H.-J.; Zhang, S.-C.; Dai, X.; Fang, Z. Quantized anomalous Hall effect in magnetic topological insulators. *Science* **2010**, *329*, 61−64.

(2) Chang, C.-Z.; Zhang, J.; Feng, X.; Shen, J.; Zhang, Z.; Guo, M.; Li, K.; Ou, Y.; Wei, P.; Wang, L.-L.; et al. Experimental observation of the quantum anomalous Hall effect in a magnetic topological insulator. *Science* **2013**, *340*, 167−170.

(3) Tokura, Y.; Yasuda, K.; Tsukazaki, A. Magnetic topological insulators. *Nature Reviews Physics* **2019**, *1*, 126−143.

(4) Deng, Y.; Yu, Y.; Shi, M. Z.; Guo, Z.; Xu, Z.; Wang, J.; Chen, X. H.; Zhang, Y. Quantum anomalous Hall effect in intrinsic magnetic topological insulator MnBi2Te4. *Science* **2020**, *367*, 895−900.

(5) Liu, C.; Wang, Y.; Li, H.; Wu, Y.; Li, Y.; Li, J.; He, K.; Xu, Y.; Zhang, J.; Wang, Y. Robust axion insulator and Chern insulator phases in a two-dimensional antiferromagnetic topological insulator. *Nature materials* **2020**, *19*, 522−527.

(6) Li, J.; Li, Y.; Du, S.; Wang, Z.; Gu, B. L.; Zhang, S. C.; He, K.; Duan, W.; Xu, Y. Intrinsic magnetic topological insulators in van der Waals layered MnBi2Te4-family materials. *Sci. Adv.* **2019**, *5*, No. eaaw5685.

(7) Mong, R. S.; Essin, A. M.; Moore, J. E. Antiferromagnetic topological insulators. *Phys. Rev. B* **2010**, *81*, No. 245209.

(8) Schaibley, J. R.; Yu, H.; Clark, G.; Rivera, P.; Ross, J. S.; Seyler, K. L.; Yao, W.; Xu, X. Valleytronics in 2D materials. *Nat. Rev. Mater.* **2016**, *1*, 16055.

(9) Otrokov, M. M.; Klimovskikh, I. I.; Bentmann, H.; Estyunin, D.; Zeugner, A.; Aliev, Z. S.; Gaß, S.; Wolter, A.; Koroleva, A.; Shikin, A. M.; et al. Prediction and observation of an antiferromagnetic topological insulator. *Nature* **2019**, *576*, 416−422.

(10) Gong, Y.; Guo, J.; Li, J.; Zhu, K.; Liao, M.; Liu, X.; Zhang, Q.; Gu, L.; Tang, L.; Feng, X.; et al. Experimental realization of an intrinsic magnetic topological insulator. *Chin. Phys. Lett.* **2019**, *36*, No. 076801.

(11) Gong, C.; Li, L.; Li, Z.; Ji, H.; Stern, A.; Xia, Y.; Cao, T.; Bao, W.; Wang, C.; Wang, Y.; et al. Discovery of intrinsic ferromagnetism in two-dimensional van der Waals crystals. *Nature* **2017**, *546*, 265−269.

(12) O'Hara, D. J.; Zhu, T.; Trout, A. H.; Ahmed, A. S.; Luo, Y. K.; Lee, C. H.; Brenner, M. R.; Rajan, S.; Gupta, J. A.; McComb, D. W.; et al. Room temperature intrinsic ferromagnetism in epitaxial manganese selenide films in the monolayer limit. *Nano Lett.* **2018**, *18*, 3125−3131.

(13) Huang, B.; Clark, G.; Navarro-Moratalla, E.; Klein, D. R.; Cheng, R.; Seyler, K. L.; Zhong, D.; Schmidgall, E.; McGuire, M. A.; Cobden, D. H.; et al. Layer-dependent ferromagnetism in a van der Waals crystal down to the monolayer limit. *Nature* **2017**, *546*, 270−273.

(14) Fei, Z.; Huang, B.; Malinowski, P.; Wang, W.; Song, T.; Sanchez, J.; Yao, W.; Xiao, D.; Zhu, X.; May, A. F.; et al. Two-dimensional itinerant ferromagnetism in atomically thin Fe3GeTe2. *Nat. Mater.* **2018**, *17*, 778−782.

(15) Lee, J.-U.; Lee, S.; Ryoo, J. H.; Kang, S.; Kim, T. Y.; Kim, P.; Park, C.-H.; Park, J.-G.; Cheong, H. Ising-type magnetic ordering in atomically thin FePS3. *Nano Lett.* **2016**, *16*, 7433−7438.

(16) Zhong, D.; Seyler, K. L.; Linpeng, X.; Cheng, R.; Sivadas, N.; Huang, B.; Schmidgall, E.; Taniguchi, T.; Watanabe, K.; McGuire, M. A.; et al. Van der Waals engineering of ferromagnetic semiconductor

heterostructures for spin and valleytronics. *Science Advances* **2017**, *3*, No. e1603113.
(17) Hasan, M. Z.; Kane, C. L. Colloquium: topological insulators. *Rev. Mod. Phys.* **2010**, *82*, 3045.
(18) Rhone, T. D.; Bhattarai, R.; Gavras, H.; Lusch, B.; Salim, M.; Mattheakis, M.; Larson, D. T.; Krockenberger, Y.; Kaxiras, E. Artificial Intelligence Guided Studies of van der Waals Magnets. *Adv. Theory Simul.* **2023**, *6*, No. 2300019.
(19) Rhone, T. D.; Chen, W.; Desai, S.; Torrisi, S. B.; Larson, D. T.; Yacoby, A.; Kaxiras, E. Data-driven studies of magnetic two-dimensional materials. *Sci. Rep.* **2020**, *10*, 15795.
(20) Xie, Y.; Tritsaris, G. A.; Granas, O.; Rhone, T. D. Data-driven studies of the magnetic anisotropy of two-dimensional magnetic materials. *J. Phys. Chem. Lett.* **2021**, *12*, 12048−12054.
(21) Otrokov, M.; Rusinov, I. P.; Blanco-Rey, M.; Hoffmann, M.; Vyazovskaya, A. Y.; Eremeev, S.; Ernst, A.; Echenique, P. M.; Arnau, A.; Chulkov, E. V. Unique thickness-dependent properties of the van der Waals interlayer antiferromagnet MnBi2Te4 films. *Phys. Rev. Lett.* **2019**, *122*, No. 107202.
(22) Zhang, D.; Shi, M.; Zhu, T.; Xing, D.; Zhang, H.; Wang, J. Topological axion states in the magnetic insulator MnBi2Te4 with the quantized magnetoelectric effect. *Phys. Rev. Lett.* **2019**, *122*, No. 206401.
(23) Zhu, T.; Bishop, A. J.; Zhou, T.; Zhu, M.; O'Hara, D. J.; Baker, A. A.; Cheng, S.; Walko, R. C.; Repicky, J. J.; Liu, T.; et al. Synthesis, magnetic properties, and electronic structure of magnetic topological insulator MnBi2Se4. *Nano Lett.* **2021**, *21*, 5083−5090.
(24) Li, P.; Yu, J.; Wang, Y.; Luo, W. Electronic structure and topological phases of the magnetic layered materials MnBi2Te4, MnBi2Se4, and MnSb2Te4. *Phys. Rev. B* **2021**, *103*, No. 155118.
(25) Zhang, H.; Yang, W.; Wang, Y.; Xu, X. Tunable topological states in layered magnetic materials of MnSb2Te4, MnBi2Se4, and MnSb2Se4. *Phys. Rev. B* **2021**, *103*, No. 094433.
(26) Djieutedjeu, H.; Makongo, J. P.; Rotaru, A.; Palasyuk, A.; Takas, N. J.; Zhou, X.; Ranmohotti, K. G.; Spinu, L.; Uher, C.; Poudeu, P. F. Crystal structure, charge transport, and magnetic properties of MnSb2Se4. *Eur. J. Inorg. Chem.* **2011**, *2011* (26), 3969−3977.
(27) Guo, S.-D.; Wang, M.-X. Predicted intrinsic piezoelectric ferromagnetism in Janus monolayer MnSbBiTe4: a first principles study. *Phys. Chem. Chem. Phys.* **2021**, *23*, 22443−22450.
(28) Wu, Z.; Xue, Y.; Shen, Z.; Song, C. Topological phase transition and skyrmions in a Janus MnSbBiSe2Te2 monolayer. *Phys. Chem. Chem. Phys.* **2022**, *25*, 96−105.
(29) You, J.-Y.; Dong, X.-J.; Gu, B.; Su, G. Electric field induced topological phase transition and large enhancements of spin-orbit coupling and Curie temperature in two-dimensional ferromagnetic semiconductors. *Phys. Rev. B* **2021**, *103*, No. 104403.
(30) Li, Y.; Xu, S.; Wang, J.; Wang, C.; Yang, B.; Lin, H.; Duan, W.; Huang, B. Interplay between quantum anomalous Hall effect and magnetic skyrmions. *Proc. Natl. Acad. Sci. U. S. A.* **2022**, *119*, No. e2122952119.
(31) Bhattarai, R.; Minch, P.; Rhone, T. D. Investigating magnetic van der Waals materials using data-driven approaches. *Journal of Materials Chemistry C* **2023**, *11*, 5601−5610.
(32) Togo, A.; Tanaka, I. First principles phonon calculations in materials science. *Scripta Materialia* **2015**, *108*, 1−5.
(33) Xue, F.; Hou, Y.; Wang, Z.; Wu, R. Two-dimensional ferromagnetic van der Waals CrCl3 monolayer with enhanced anisotropy and Curie temperature. *Physical review b* **2019**, *100*, No. 224429.
(34) Jansen, H. Magnetic anisotropy in density-functional theory. *Phys. Rev. B* **1999**, *59*, 4699.
(35) Li, B.; Yan, J.-Q.; Pajerowski, D. M.; Gordon, E.; Nedić, A.-M.; Sizyuk, Y.; Ke, L.; Orth, P. P.; Vaknin, D.; McQueeney, R. J. Competing magnetic interactions in the antiferromagnetic topological insulator MnBi 2 Te 4. *Physical review letters* **2020**, *124*, No. 167204.
(36) Leonov, A.; Mostovoy, M. Multiply periodic states and isolated skyrmions in an anisotropic frustrated magnet. *Nat. Commun.* **2015**, *6*, 8275.
(37) Riberolles, S. X.; Zhang, Q.; Gordon, E.; Butch, N. P.; Ke, L.; Yan, J.-Q.; McQueeney, R. J. Evolution of magnetic interactions in Sb-substituted MnBi 2 Te 4. *Phys. Rev. B* **2021**, *104*, No. 064401.
(38) Wang, Y.; Wang, C.; Liang, S.; Ma, Z.; Xu, K.; Liu, X.; Zhang, L.; Admasu, A. S.; Cheong, S.; Wang, L.; Chen, M.; Liu, Z.; Cheng, B.; Ji, W.; Miao, F.; et al. Strain-sensitive magnetization reversal of a van der Waals magnet. *Adv. Mater.* **2020**, *32*, No. 2004533.
(39) Xue, F.; Wang, Z.; Hou, Y.; Gu, L.; Wu, R. Control of magnetic properties of MnBi2Te4 using a van der Waals ferroelectric III2-VI3 film and biaxial strain. *Phys. Rev. B* **2020**, *101*, No. 184426.
(40) Minch, P.; Bhattarai, R.; Rhone, T. D. Data-driven study of magnetic anisotropy in transition metal dichalcogenide monolayers. *Solid State Commun.* **2023**, *371*, No. 115248.
(41) Wang, Z.; Zhang, M.; Ge, Y.; Wan, W.; Liu, Y. Monolayer MX2 (M = Cr, Mn; X = Se, Te) with a square lattice: A ferromagnetic half-metal with high Curie temperature. *Results in Physics* **2023**, *51*, No. 106687.
(42) Kvashnin, Y.; Bergman, A.; Lichtenstein, A.; Katsnelson, M. Relativistic exchange interactions in CrX3 (X = Cl, Br, I) monolayers. *Phys. Rev. B* **2020**, *102*, No. 115162.
(43) Torelli, D.; Thygesen, K. S.; Olsen, T. High throughput computational screening for 2D ferromagnetic materials: the critical role of anisotropy and local correlations. *2D Materials* **2019**, *6*, No. 045018.
(44) Dong, X.-J.; You, J.-Y.; Gu, B.; Su, G. Strain-induced room-temperature ferromagnetic semiconductors with large anomalous Hall conductivity in two-dimensional Cr2Ge2Se6. *Physical Review Applied* **2019**, *12*, No. 014020.
(45) Sivadas, N.; Daniels, M. W.; Swendsen, R. H.; Okamoto, S.; Xiao, D. Magnetic ground state of semiconducting transition-metal trichalcogenide monolayers. *Phys. Rev. B* **2015**, *91*, No. 235425.
(46) Bhattarai, R.; Minch, P.; Liang, Y.; Zhang, S.; Rhone, T. D. Strain-induced topological phase transition in ferromagnetic Janus monolayer MnSbBiS2Te2. *Phys. Chem. Chem. Phys.* **2024**, *26*, 10111−10119.
(47) Ramzan, M. S.; Bacic, V.; Jing, Y.; Kuc, A. Electronic properties of a new family of layered materials from groups 14 and 15: first-principles simulations. *J. Phys. Chem. C* **2019**, *123*, 25470−25476.
(48) Ding, Y.; Wang, Y. Hydrogen-induced stabilization and tunable electronic structures of penta-silicene: a computational study. *Journal of Materials Chemistry C* **2015**, *3*, 11341−11348.
(49) Badalov, S. V.; Yagmurcukardes, M.; Peeters, F. M.; Sahin, H. Enhanced stability of single-layer w-gallenene through hydrogenation. *J. Phys. Chem. C* **2018**, *122*, 28302−28309.
(50) Medina, D. B.; Salomon, E.; Le Lay, G.; Angot, T. Hydrogenation of silicene films grown on Ag(111). *J. Electron Spectrosc. Relat. Phenom.* **2017**, *219*, 57−62.
(51) Yao, Q.; Zhang, L.; Kabanov, N.; Rudenko, A.; Arjmand, T.; Rahimpour Soleimani, H.; Klavsyuk, A.; Zandvliet, H. Bandgap opening in hydrogenated germanene. *Appl. Phys. Lett.* **2018**, *112*, 171607.
(52) Tang, W.; Chen, H.; Su, Y.; Niu, X. Computational screening of two-dimensional substrates for stabilizing honeycomb borophene. *Appl. Surf. Sci.* **2023**, *615*, No. 156388.
(53) Otero-Martínez, C.; Fiuza-Maneiro, N.; Polavarapu, L. Enhancing the intrinsic and extrinsic stability of halide perovskite nanocrystals for efficient and durable optoelectronics. *ACS Appl. Mater. Interfaces* **2022**, *14*, 34291−34302.
(54) Wang, X.; Sun, Y.; Liu, K. Chemical and structural stability of 2D layered materials. *2D Materials* **2019**, *6*, No. 042001.
(55) Chang, Z.-W.; Xu, J.-J.; Liu, Q.-C.; Li, L.; Zhang, X.-B. Recent progress on stability enhancement for cathode in rechargeable non-aqueous lithium-oxygen battery. *Adv. Energy Mater.* **2015**, *5*, No. 1500633.
(56) Gou, J.; Xia, B.; Li, H.; Wang, X.; Kong, L.; Cheng, P.; Li, H.; Zhang, W.; Qian, T.; Ding, H.; et al. Binary two-dimensional

https://doi.org/10.1021/acsami.4c12946
ACS Appl. Mater. Interfaces 2024, 16, 60856−60864

honeycomb lattice with strong spin-orbit coupling and electron-hole asymmetry. *Phys. Rev. Lett.* **2018**, *121*, No. 126801.
(57) Ding, Y.; Wang, Y. Stabilizing the isolated Sn2 Bi nanosheet and tailoring its electronic structure by chemical functionalization: a computational study. *Appl. Phys. Lett.* **2019**, *114*, No. 073103.
(58) Peng, J.; Zhuang, C.; Gu, H.; Zhu, L.; Zhang, T. How can the unstable two-dimensional Sn2 Bi be experimentally realized on Si(111)? *J. Nanopart. Res.* **2022**, *24*, 72.
(59) Shu, H. Hydrogenation-induced interfacial bonding effects on the structural, electronic, and optical properties of GaN bilayer. *Vacuum* **2023**, *213*, No. 112080.
(60) Dudarev, S. L.; Botton, G. A.; Savrasov, S. Y.; Humphreys, C.; Sutton, A. P. Electron-energy-loss spectra and the structural stability of nickel oxide: An LSDA+U study. *Phys. Rev. B* **1998**, *57*, 1505.
(61) Heyd, J.; Scuseria, G. E.; Ernzerhof, M. Hybrid functionals based on a screened Coulomb potential. *J. Chem. Phys.* **2003**, *118*, 8207−8215.
(62) Heyd, J.; Scuseria, G. E. Efficient hybrid density functional calculations in solids: Assessment of the Heyd−Scuseria−Ernzerhof screened Coulomb hybrid functional. *J. Chem. Phys.* **2004**, *121*, 1187−1192.
(63) Hedin, L. New method for calculating the one-particle Green's function with application to the electron-gas problem. *Phys. Rev.* **1965**, *139*, A796.
(64) Hybertsen, M. S.; Louie, S. G. Electron correlation in semiconductors and insulators: Band gaps and quasiparticle energies. *Phys. Rev. B* **1986**, *34*, 5390.
(65) Onida, G.; Reining, L.; Rubio, A. Electronic excitations: density-functional versus many-body Green's-function approaches. *Reviews of modern physics* **2002**, *74*, 601.
(66) Rohlfing, M.; Louie, S. G. Electron-hole excitations in semiconductors and insulators. *Physical review letters* **1998**, *81*, 2312.
(67) Albrecht, S.; Reining, L.; Del Sole, R.; Onida, G. Ab initio calculation of excitonic effects in the optical spectra of semiconductors. *Physical review letters* **1998**, *80*, 4510.
(68) An, Y.; Wang, K.; Gong, S.; Hou, Y.; Ma, C.; Zhu, M.; Zhao, C.; Wang, T.; Ma, S.; Wang, H.; et al. Nanodevices engineering and spin transport properties of MnBi2Te4 monolayer. *npj Comput. Mater.* **2021**, *7*, 45.
(69) Li, Z.; Li, J.; He, K.; Wan, X.; Duan, W.; Xu, Y. Tunable interlayer magnetism and band topology in van der Waals heterostructures of Mn Bi 2 Te 4-family materials. *Phys. Rev. B* **2020**, *102*, No. 081107.
(70) Bao, L.; He, L.; Meyer, N.; Kou, X.; Zhang, P.; Chen, Z.-G.; Fedorov, A. V.; Zou, J.; Riedemann, T. M.; Lograsso, T. A.; et al. Weak anti-localization and quantum oscillations of surface states in topological insulator Bi2Se2Te. *Sci. Rep.* **2012**, *2*, 726.
(71) Martínez-Velarte, M. C.; Kretz, B.; Moro-Lagares, M.; Aguirre, M. H.; Riedemann, T. M.; Lograsso, T. A.; Morellon, L.; Ibarra, M. R.; Garcia-Lekue, A.; Serrate, D. Chemical disorder in topological insulators: a route to magnetism tolerant topological surface states. *Nano Lett.* **2017**, *17*, 4047−4054.
(72) Choi, H.; Kim, T. H.; Chae, J.; Baeck, J.; Kee, C.-S.; Jeong, K.-H.; Jeong, H.-S.; Kang, C.; Cho, M.-H. Evolution of the surface state in Bi 2 Se 2 Te thin films during phase transition. *Nanoscale* **2015**, *7*, 14924−14936.
(73) Zou, X.; Yuan, X.; Liang, L.; Tian, F.; Li, Y.; Sun, Y.; Wang, C. Unusual Janus Bi2TeSe2 Topological Insulators Displaying Second-Harmonic Generation, Linear-in-Temperature Resistivity, and Weak Antilocalization. *J. Am. Chem. Soc.* **2024**, *146*, 17784−17792.
(74) Lu, Z.; Wu, Y.; Xu, Y.; Ma, C.; Chen, Y.; Xu, K.; Zhang, H.; Zhu, H.; Fang, Z. Ultrahigh electron mobility induced by strain engineering in direct semiconductor monolayer Bi 2 TeSe 2. *Nanoscale* **2019**, *11*, 20620−20629.
(75) Kresse, G.; Furthmüller, J. Efficient iterative schemes for ab initio total-energy calculations using a plane-wave basis set. *Phys. Rev. B* **1996**, *54*, 11169.
(76) Blöchl, P. E. Projector augmented-wave method. *Physical Beview B* **1994**, *50*, 17953.
(77) Perdew, J. P.; Burke, K.; Ernzerhof, M. Generalized gradient approximation made simple. *Phys. Rev. Lett.* **1996**, *77*, 3865.
(78) Gresch, D.; Autes, G.; Yazyev, O. V.; Troyer, M.; Vanderbilt, D.; Bernevig, B. A.; Soluyanov, A. A. Z2Pack: Numerical implementation of hybrid Wannier centers for identifying topological materials. *Phys. Rev. B* **2017**, *95*, No. 075146.
(79) Wu, Q.; Zhang, S.; Song, H.-F.; Troyer, M.; Soluyanov, A. A. WannierTools: An open-source software package for novel topological materials. *Comput. Phys. Commun.* **2018**, *224*, 405−416.

https://doi.org/10.1021/acsami.4c12946
ACS Appl. Mater. Interfaces 2024, 16, 60856−60864